Nurminen, Tuure; Mourouvin, Rayane; Hinkkanen, Marko; Kukkola, Jarno; Routimo, Mikko; Vilhunen, Antti; Harnefors, Lennart

Observer-based power-synchronization control for grid-forming converters

Published in:
2023 IEEE Belgrade PowerTech

DOI:
10.1109/PowerTech55446.2023.10202897

Published: 29/06/2023

Document Version
Peer-reviewed accepted author manuscript, also known as Final accepted manuscript or Post-print

Please cite the original version:
Nurminen, T., Mourouvin, R., Hinkkanen, M., Kukkola, J., Routimo, M., Vilhunen, A., & Harnefors, L. (2023). Observer-based power-synchronization control for grid-forming converters. In *2023 IEEE Belgrade PowerTech* (pp. 1-6). Article 10202897 IEEE. https://doi.org/10.1109/PowerTech55446.2023.10202897

Observer-Based Power-Synchronization Control for Grid-Forming Converters

Tuure Nurminen
Aalto University
Espoo, Finland
tuure.nurminen@aalto.fi

Rayane Mourouvin
Aalto University
Espoo, Finland
rayane.mourouvin@aalto.fi

Marko Hinkkanen
Aalto University
Espoo, Finland
marko.hinkkanen@aalto.fi

Jarno Kukkola
ABB Oy Drives
Helsinki, Finland
jarno.kukkola1@fi.abb.com

Mikko Routimo
ABB Oy Drives
Helsinki, Finland
mikko.routimo@fi.abb.com

Antti Vilhunen
ABB Oy Drives
Helsinki, Finland
antti.vilhunen@fi.abb.com

Lennart Harnefors
ABB Corporate Research
Västerås, Sweden
lennart.harnefors@se.abb.com

***Abstract*—This paper proposes an observer-based power-synchronization control (OPSC) method for grid-forming converters. The method can also be utilized for the starting of synchronous generators. It is analogous to observer-based volts-per-hertz (V/Hz) control of electric machine drives, consisting of state-feedback control and an observer. A linearized model of the closed-loop system is derived, passivity of the mechanical subsystem is studied and tuning recommendations are given. The power tracking performance is assessed and compared to that of reference-feedforward power-synchronization control (RFPSC) with the help of simulations and laboratory experiments using a 12.5-kVA converter. The results show that the proposed control method provides good performance in both weak and strong grids.**

***Index Terms*—Grid-forming converter, observer, power-synchronization control (PSC), stability, state feedback.**

I. Introduction

Grid-forming converters are a potential solution to many stability issues seen in grids experiencing high penetration of converter-interfaced energy sources [1]–[4]. In contrast to conventional grid-following converters, the grid-forming converters make use of their own voltage and frequency references to create a stable grid voltage without having to rely on synchronous generators [5]. Their capability to self-synchronize allows for superior performance in weak grids. This is beneficial since renewable energy sources may be built in remote locations characterised by weak grid conditions [2]. Grid-forming converters also have the capability to take part in re-starting the grid following a blackout [6]–[8], which is not possible with conventional grid-following converters.

Many control methods have been developed for grid-forming converters, e.g., droop-based methods [9], [10], and virtual synchronous generators [11], [12]. Power-synchronization control (PSC) is an established control method for grid-forming converters. Conventional PSC [13], [14] has good performance in weak grids while reference-feedforward PSC (RFPSC) [15] also functions well in strong grids.

This paper proposes an observer-based PSC (OPSC) method for grid-forming converters. OPSC is developed based on a grid model utilizing virtual flux linkages. The method consists of a state-feedback control law, an observer for estimating virtual flux linkage and torque, and a power-synchronization loop. Tuning recommendations for the method are developed and the resulting good performance is shown through simulations and experimental results.

Rather than trying to emulate the behaviour of a synchronous machine, the control method is instead analogous to observer-based V/Hz control of electric machine drives [16]. Therefore, reference variables that are familiar from machine drives are used, e.g. flux linkage and torque, but these can be easily converted to terms commonly used with grid converters. The method inherently provides electric machine control capability, which makes it possible to power a synchronous generator from zero-voltage and zero-speed conditions.

II. Grid Model

This paper utilizes column vector notation to present space vectors, e.g., the converter voltage is $\boldsymbol{u}_\mathrm{c} = [u_\mathrm{cd}, u_\mathrm{cq}]^\mathrm{T}$. The orthogonal rotation matrix is $\boldsymbol{J} = \left[\begin{smallmatrix} 0 & -1 \\ 1 & 0 \end{smallmatrix}\right]$, the identity matrix is $\boldsymbol{I} = \left[\begin{smallmatrix} 1 & 0 \\ 0 & 1 \end{smallmatrix}\right]$, and the zero matrix is $\mathbf{0}_{m,n}$ with the dimensions given in the subscript.

For describing OPSC, it is convenient to consider the grid voltage to be created by a (virtual) synchronous machine, whose stator resistance is negligible and stator inductance is L. The grid angle ϑ_g and angular frequency $\omega_\mathrm{g} = \mathrm{d}\vartheta_\mathrm{g}/\mathrm{d}t$ correspond to the rotor angle and angular speed, respectively, of the virtual machine. Correspondingly, the grid voltage $\boldsymbol{e}_\mathrm{g}$ is the induced voltage due to rotation of the magnetized rotor.

Fig. 1 shows the grid model in stationary coordinates. This model in controller (or general) coordinates, rotating at the

This project has been sponsored by ABB Oy and by the Academy of Finland Centre of Excellence in *High-Speed Electromechanical Energy Conversion Systems.*

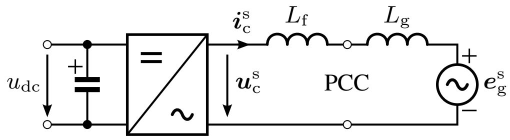

Fig. 1. Converter and grid models with space vector notation in a stationary coordinates, indicated by the superscript s. PCC marks the point of common coupling.

angular speed ω_c, is given by

$$\frac{\mathrm{d}\boldsymbol{\psi}_\mathrm{c}}{\mathrm{d}t} = \boldsymbol{u}_\mathrm{c} - \boldsymbol{J}\omega_\mathrm{c}\boldsymbol{\psi}_\mathrm{c} \tag{1a}$$

$$\boldsymbol{i}_\mathrm{c} = \frac{\boldsymbol{\psi}_\mathrm{c} - \boldsymbol{\psi}_\mathrm{g}}{L} \tag{1b}$$

where $L = L_\mathrm{f} + L_\mathrm{g}$ is the sum of the filter and grid inductances and $\boldsymbol{\psi}_\mathrm{c}$ is the virtual converter flux linkage. The grid flux linkage is

$$\boldsymbol{\psi}_\mathrm{g} = \mathrm{e}^{-\boldsymbol{J}\delta}\boldsymbol{\psi}_\mathrm{g}^\mathrm{g} \tag{2}$$

where $\boldsymbol{\psi}_\mathrm{g}^\mathrm{g} = [0, -\psi_\mathrm{g}]^\mathrm{T}$ is the grid flux linkage in grid coordinates and ψ_g is constant. Here, the direction of $\boldsymbol{\psi}_\mathrm{g}^\mathrm{g}$ is selected such that the d-axis of the grid coordinate system is along the induced grid voltage $\boldsymbol{e}_\mathrm{g}^\mathrm{g} = \boldsymbol{J}\omega_\mathrm{g}\boldsymbol{\psi}_\mathrm{g}^\mathrm{g}$. The angle $\delta = \vartheta_\mathrm{c} - \vartheta_\mathrm{g}$, where ϑ_c is the angle of the controller coordinate system with respect to the stationary frame, corresponds to the load angle. Its dynamic equation is

$$\frac{\mathrm{d}\delta}{\mathrm{d}t} = \omega_\mathrm{c} - \omega_\mathrm{g} \tag{3}$$

Using the synchronous machine analogy, we define a virtual electromagnetic torque

$$\tau_\mathrm{g} = \boldsymbol{i}_\mathrm{c}^\mathrm{T}\boldsymbol{J}\boldsymbol{\psi}_\mathrm{c} \tag{4}$$

where per-unit quantities are assumed. The mechanical power fed to this synchronous machine is $p_\mathrm{g} = \tau_\mathrm{g}\omega_\mathrm{g}$. To further continue this analogy, the equation of motion is

$$J_\mathrm{g}\frac{\mathrm{d}\omega_\mathrm{g}}{\mathrm{d}t} = \tau_\mathrm{g} - \tau_\mathrm{m} \tag{5}$$

where J_g is the virtual moment of inertia and τ_m is the virtual mechanical torque applied to the rotor by the prime mover. This equation of motion yields the power balance (also known as the swing equation) when both sides are multiplied by ω_g.

III. Control System

Fig. 2 shows the control structure of the proposed OPSC method. It consists of a state-feedback control law, an observer for estimating flux and torque, and a power-synchronization loop.

A. Control Law

The converter voltage reference is obtained with state-feedback control

$$\boldsymbol{u}_\mathrm{c,ref} = \boldsymbol{J}\omega_\mathrm{c}\hat{\boldsymbol{\psi}}_\mathrm{c} + \alpha_\psi(\boldsymbol{\psi}_\mathrm{c,ref} - \hat{\boldsymbol{\psi}}_\mathrm{c}) \tag{6}$$

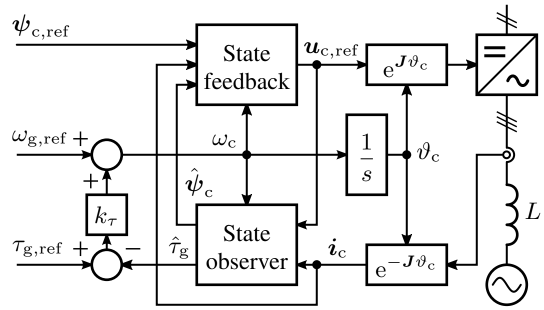

Fig. 2. OPSC of a grid converter.

where $\boldsymbol{\psi}_\mathrm{c,ref} = -\boldsymbol{J}\boldsymbol{u}_\mathrm{ref}/\omega_\mathrm{g,ref}$ is the converter flux reference, $\boldsymbol{u}_\mathrm{ref} = [u_\mathrm{ref}, 0]^\mathrm{T}$ is the reference for the converter output voltage, $\omega_\mathrm{g,ref}$ is the grid angular frequency reference (normally chosen to be equal to the nominal grid frequency), $\hat{\boldsymbol{\psi}}_\mathrm{c}$ is the converter flux estimate, and α_ψ is the flux-control bandwidth. The control law has similarities with the one proposed for synchronous machine drives in [16].

The converter frequency reference is

$$\frac{\mathrm{d}\vartheta_\mathrm{c}}{\mathrm{d}t} = \omega_\mathrm{c} = \omega_\mathrm{g,ref} + k_\tau(\tau_\mathrm{g,ref} - \hat{\tau}_\mathrm{g}) \tag{7}$$

where $\tau_\mathrm{g,ref} = p_\mathrm{g,ref}/\omega_\mathrm{g,ref}$ is the torque reference obtained by scaling the power reference $p_\mathrm{g,ref}$, $\hat{\tau}_\mathrm{g}$ is the estimate of the virtual torque, and k_τ is the torque-synchronization gain. It is interesting to note that (7) is similar to the expression of the converter frequency in conventional PSC and RFPSC [14], [15], the only difference being that they use active power whereas OPSC uses virtual torque. To achieve comparable performance to RFPSC, the synchronization loops of OPSC and RFPSC are tuned similarly by selecting $k_\tau = \omega_\mathrm{g,ref}k_\mathrm{p}$, where $k_\mathrm{p} = \omega_\mathrm{g,ref}R_\mathrm{a}/u_\mathrm{ref}$ is the power-synchronization loop gain used for RFPSC and R_a is the active resistance [15].

Alternatively, the control law (6) can be expressed as

$$\boldsymbol{u}_\mathrm{c,ref} = \boldsymbol{J}\omega_\mathrm{c}\hat{\boldsymbol{\psi}}_\mathrm{c} + \alpha_\psi\hat{L}\left(\boldsymbol{i}_\mathrm{c,ref} - \boldsymbol{i}_\mathrm{c}\right) \tag{8a}$$

where $\hat{L}$ is an estimate of the total grid inductance. The internal reference signal

$$\boldsymbol{i}_\mathrm{c,ref} = \boldsymbol{i}_\mathrm{c} + \frac{\boldsymbol{\psi}_\mathrm{c,ref} - \hat{\boldsymbol{\psi}}_\mathrm{c}}{\hat{L}} \tag{8b}$$

can be saturated in order to provide some current limitation functionality. Thus, (8) enables the implementation of, e.g., the current limitation schemes described in [17]–[19]. When $\boldsymbol{i}_\mathrm{c,ref}$ is not saturated, the control law (8) is equivalent to (6).

B. State Observer

The observer used in this paper is based on previous work on flux observers [16], [20], used in motor drive applications.

The estimated flux and torque dynamics are

$$\frac{\mathrm{d}\hat{\boldsymbol{\psi}}_\mathrm{c}}{\mathrm{d}t} = \boldsymbol{u}_\mathrm{c} - \boldsymbol{J}\omega_\mathrm{c}\hat{\boldsymbol{\psi}}_\mathrm{c} + \frac{\alpha_\mathrm{o}\hat{\boldsymbol{\psi}}_\mathrm{g}}{\|\hat{\boldsymbol{\psi}}_\mathrm{g}\|}\left(\psi_\mathrm{g,ref} - \|\hat{\boldsymbol{\psi}}_\mathrm{g}\|\right) \tag{9a}$$

$$\hat{\boldsymbol{\psi}}_\mathrm{g} = \hat{\boldsymbol{\psi}}_\mathrm{c} - \hat{L}\boldsymbol{i}_\mathrm{c} \tag{9b}$$

$$\hat{\tau}_\mathrm{g} = \boldsymbol{i}_\mathrm{c}^\mathrm{T}\boldsymbol{J}\hat{\boldsymbol{\psi}}_\mathrm{c} \tag{9c}$$

where $\psi_\mathrm{g,ref} = u_\mathrm{g,ref}/\omega_\mathrm{g,ref}$ is a constant. The signal $\boldsymbol{u}_\mathrm{c}$ used in (9) is an estimate of the realized voltage, with compensations for the time delays, $\boldsymbol{u}_\mathrm{c}(t) = \boldsymbol{u}_\mathrm{c,ref}(t - T_\mathrm{d})\exp(-\boldsymbol{J}\omega_\mathrm{c}T_\mathrm{d})$, where T_d is the total delay [21]. This realized voltage is typically available from the pulse-width modulator (PWM), thus not requiring any additional voltage sensor. The observer gain α_o dictates the impact of the error term that is dependent on the grid inductance. Selecting a small observer gain in relation to grid frequency, e.g. $\alpha_\mathrm{o} = 0.1\ldots0.2$ p.u., makes the observer robust to parametrization errors in total inductance $\hat{L}$.

IV. Analysis

A linear model of the system is derived for stability analysis (cf. the Appendix). For linearization, operating point quantities are marked with subscript 0 and small-signal perturbations are marked with a preceding Δ, e.g., $\boldsymbol{i}_\mathrm{c} = \boldsymbol{i}_\mathrm{c0} + \Delta\boldsymbol{i}_\mathrm{c}$.

The closed-loop transfer function from the flux reference to the converter flux results in a first-order system,

$$\Delta\boldsymbol{\psi}_\mathrm{c} = \frac{\alpha_\psi}{s + \alpha_\psi}\Delta\boldsymbol{\psi}_\mathrm{c,ref} \tag{10}$$

The range of α_ψ that results in good performance is wide and thus its selection is not of critical importance.

Fig. 3 presents the virtual mechanical subsystem, where the open-loop mechanics of the virtual machine are described by the equation of motion in (5). The transfer function from the controller angular frequency $\Delta\omega_\mathrm{c}$ to the output torque $\Delta\tau_\mathrm{g}$ of the converter is

$$G_\mathrm{m}(s) = \frac{\boldsymbol{\psi}_\mathrm{c0}^\mathrm{T}\boldsymbol{\psi}_\mathrm{g0}}{sL} \tag{11}$$

which is passive due to $\mathrm{Re}\{G_\mathrm{m}(\mathrm{j}\omega)\} \geq 0$ for any $\omega \in \mathbb{R}$. The torque estimate is $\Delta\hat{\tau}_\mathrm{g} = \Delta\tau_\mathrm{g} - \boldsymbol{i}_\mathrm{c0}^\mathrm{T}\boldsymbol{J}\Delta\tilde{\boldsymbol{\psi}}_\mathrm{c}$, where the converter flux estimation error $\Delta\tilde{\boldsymbol{\psi}}_\mathrm{c}$ is independent of $\Delta\omega_\mathrm{c}$. The only remaining component in the synchronization loop is the gain k_τ, which is positive. Thus, the whole closed-loop mechanical subsystem is guaranteed to be passive for passive open-loop mechanics. This result holds not only with (5) but with any passive mechanics, such as a two-mass system. This feature allows the grid-forming converter to be used in some special applications, where, e.g., starting of a synchronous machine is needed.

V. Simulation Results

A. Power Tracking Performance

The performance of RFPSC and OPSC is compared through simulations. Table I provides the parameter values. RFPSC is tuned according to the guidelines given in [14], [15].

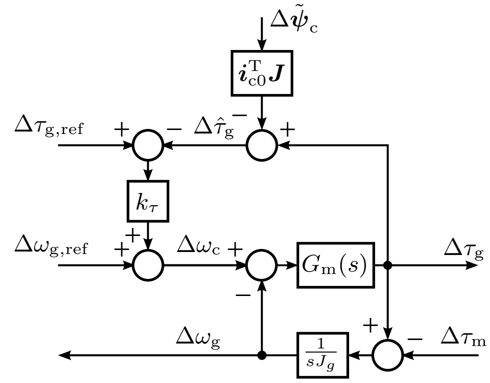

Fig. 3. Linearized virtual mechanical subsystem with the virtual machine mechanics represented by the equation of motion (5).

TABLE I
Parameters Used in the Grid Simulations and Experiments

Parameters	Actual value	Per-unit value
System		
Rated voltage	$\sqrt{2/3}\cdot 400$ V	1 p.u.
Rated current	$\sqrt{2}\cdot 18$ A	1 p.u.
Rated power	12.5 kVA	1 p.u.
DC-bus voltage	650 V	2 p.u.
Fundamental frequency	50 Hz	1 p.u.
Switching frequency	4 kHz	80 p.u.
Sampling frequency	8 kHz	160 p.u.
Filter inductance L_f	6.3 mH	0.15 p.u.
Tuning		
Active resistance R_a	2.6 Ω	0.2 p.u.
Filter bandwidth ω_b [15]	$2\pi\cdot 5$ rad/s	0.1 p.u.
State-feedback gain α_ψ	$2\pi\cdot 120$ rad/s	2.4 p.u.
Observer gain α_o	$2\pi\cdot 10$ rad/s	0.2 p.u.

Strong and weak grid conditions are tested, corresponding to $L_\mathrm{g} = 0$ p.u. and $L_\mathrm{g} = 0.85$ p.u., respectively. In both cases OPSC is tuned with $\hat{L} = L_\mathrm{f}$, which will result in a parameter error when the grid inductance is nonzero.

The simulation results for RFPSC and OPSC are shown in Figs. 4 and 5, respectively. The power, current, and voltage responses to step changes in the active power reference are plotted. Both methods display nearly identical behaviour in the strong grid condition, where $\hat{L} = L_\mathrm{f} = L$ is accurate.

In the weak grid condition, the parameter error in OPSC becomes large, i.e., the actual inductance is $L = L_\mathrm{f} + L_\mathrm{g}$ while its estimate is $\hat{L} = L_\mathrm{f}$. Good performance is still achieved due to a low value of α_o, reducing the impact of the parameter error. On the other hand, low α_o also results in slower convergence and, thus, a small degree of ringing after the step changes as well as lower delivered reactive power, cf. Fig. 5. If an estimate for the grid inductance L_g were added to $\hat{L}$, the observer gain α_o could be selected higher without risking stability.

B. Starting a Synchronous Generator

The starting of a synchronous generator with OPSC is studied through simulations. The parameters of a 2-MW four-

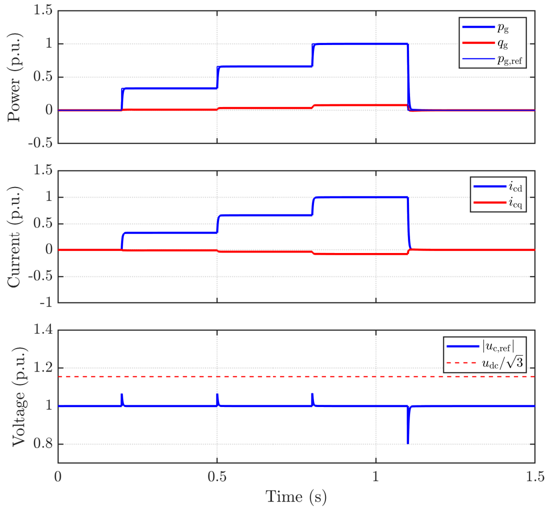

(a)

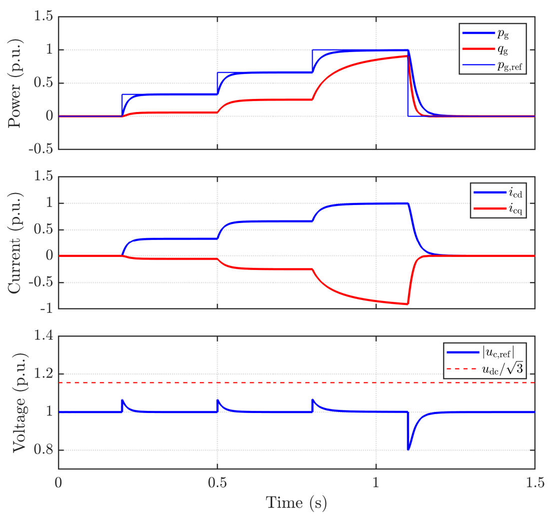

(b)

Fig. 4. Step responses for RFPSC: (a) strong grid ($L_g = 0$ p.u.); (b) weak grid ($L_g = 0.85$ p.u.)

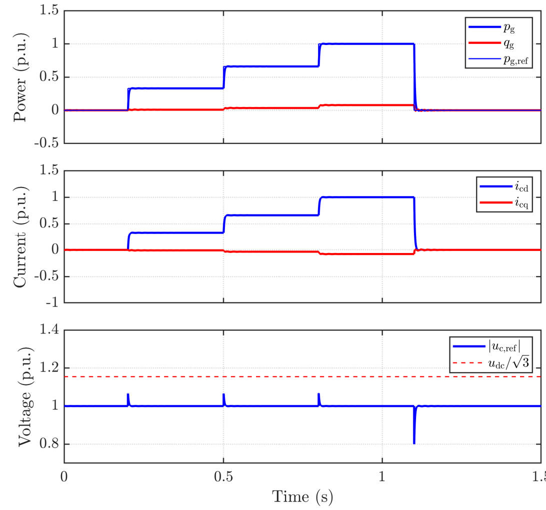

(a)

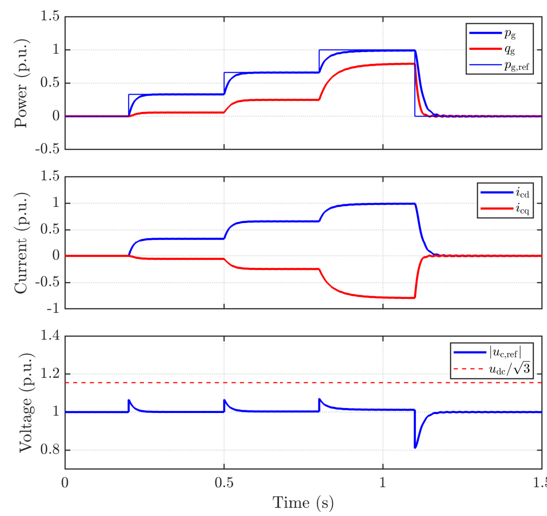

(b)

Fig. 5. Step responses for OPSC: (a) strong grid ($L_g = 0$ p.u.); (b) weak grid ($L_g = 0.85$ p.u.)

pole permanent-magnet (PM) synchronous generator are given in Table II. The converter has a power rating of 600 kW.

The per-unit tuning parameter values given in Table I are also used in this simulation. The reference flux is $\psi_{c,ref} = 1$ p.u. and the inductance estimate is $\hat{L} = L_d$. The simulation results are shown in Fig. 6. The synchronous generator is accelerated from zero speed to the rated value under no-load conditions by ramping up the frequency reference over a period of 30 seconds, which keeps the current magnitude below 1 p.u.

VI. Experimental Results

A. Laboratory Setup

The performance of OPSC is studied experimentally. The same parameters and tuning apply as in the simulations, cf. Table I. Fig. 7 presents a block diagram of the laboratory setup, consisting of two 12.5-kVA three-phase converters. The first converter is used to supply power to the DC-bus from the grid, thus acting as a source. The second converter is used to supply power to the grid, utilizing the control method under test. A dSPACE MicroLabBox is utilized for control of the second converter and also for monitoring purposes. A 50-kVA four-quadrant three-phase programmable grid simulator from Regatron is placed at the output of the test converter.

B. Power Tracking

OPSC is evaluated with two different levels of grid inductance, $L_g = 0$ p.u. and $L_g = 0.62$ p.u. The same power reference sequence is used as in the simulations. The experimental results for power tracking, shown in Fig. 8, confirm the results obtained from the simulations. It shows that OPSC works well in both strong and weak grids.

TABLE II
PARAMETERS USED IN SIMULATION OF STARTING A 2-MW FOUR-POLE PM SYNCHRONOUS GENERATOR

Parameters	Actual value	Per-unit value
600-kW converter		
Rated voltage	$\sqrt{2/3}\cdot 400$ V	1 p.u.
Rated current	$\sqrt{2}\cdot 1.22$ kA	1 p.u.
DC-bus voltage	650 V	2 p.u.
Fundamental frequency	50 Hz	1 p.u.
2-MW generator		
Rated voltage	$\sqrt{2/3}\cdot 400$ V	1 p.u.
Rated current	$\sqrt{2}\cdot 4.08$ kA	3.34 p.u.
Rated speed	1 500 r/min	1 p.u.
Stator resistance R_s	0.76 mΩ	0.003 p.u.
d-axis inductance L_d	0.52 mH	0.62 p.u.
q-axis inductance L_q	0.52 mH	0.62 p.u.
PM flux linkage ψ_f	0.55 Vs	0.53 p.u.
Moment of inertia J	324 kgm^2	16 800 p.u.

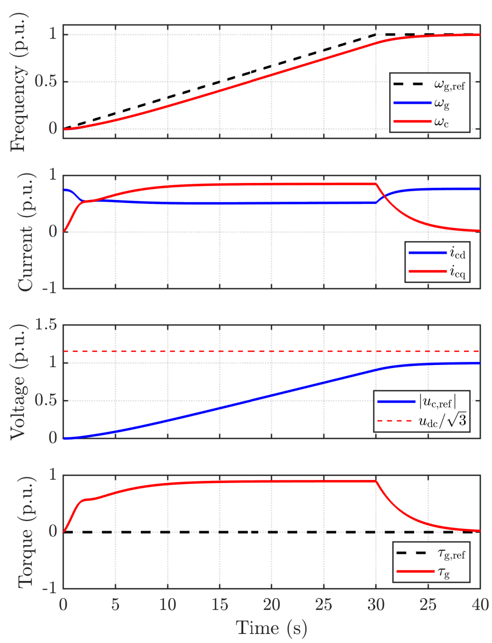

Fig. 6. Starting a 2-MW synchronous generator with OPSC.

VII. CONCLUSIONS

An OPSC method was developed for the control of grid-forming converters. Converter flux dynamics and mechanical passivity was analysed based on the linearized model of the closed-loop system. The tuning recommendations that were developed makes the method robust against parameter uncertainty and allows the same tuning to be used regardless of grid strength. Based on the test results, the method shows good power tracking performance in both weak and strong grids. Simultaneously, the active power tracking can be seen to be very similar to that of RFPSC. Results show that the use of flux linkages in the control law also enables OPSC to easily start a synchronous generator.

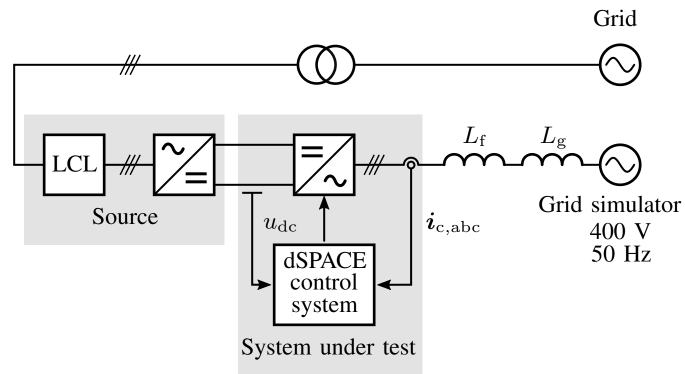

Fig. 7. Experimental setup. L_g is used only in the weak-grid condition.

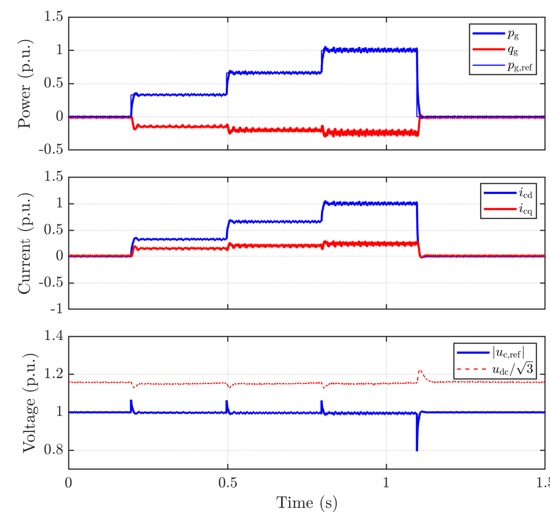

(a)

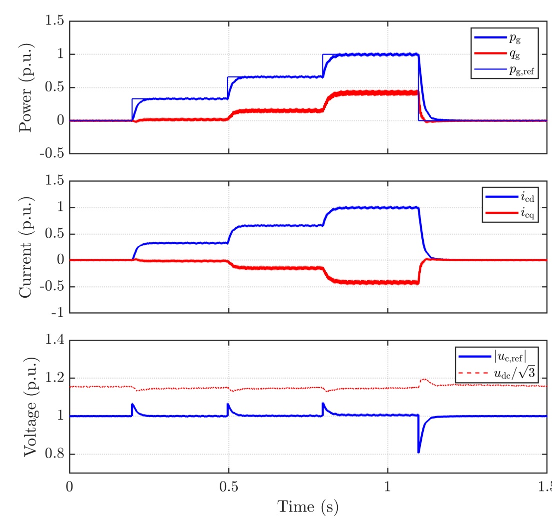

(b)

Fig. 8. Experimental results for power tracking with OPSC: (a) strong grid ($L_\mathrm{g} = 0$ p.u.); (b) weak grid ($L_\mathrm{g} = 0.62$ p.u.)

APPENDIX
LINEARIZED MODEL

Let us assume accurate converter voltage $\boldsymbol{u}_\mathrm{c} = \boldsymbol{u}_\mathrm{c,ref}$ and inductance estimate $\hat{L} = L$. The linearized form of the control law (6) is

$$\Delta \boldsymbol{u}_{\mathrm{c}} = \boldsymbol{J}\omega_{\mathrm{c0}}\Delta\hat{\boldsymbol{\psi}}_{\mathrm{c}} + \boldsymbol{J}\boldsymbol{\psi}_{\mathrm{c0}}\Delta\omega_{\mathrm{c}} + \alpha_{\psi}(\Delta\boldsymbol{\psi}_{\mathrm{c,ref}} - \Delta\hat{\boldsymbol{\psi}}_{\mathrm{c}}) \tag{12}$$

Then, (12) is inserted in the linearized form of (1a), giving

$$\frac{\mathrm{d}\Delta\boldsymbol{\psi}_{\mathrm{c}}}{\mathrm{d}t} = -\alpha_{\psi}\Delta\boldsymbol{\psi}_{\mathrm{c}} + (\alpha_{\psi}\boldsymbol{I} - \boldsymbol{J}\omega_{\mathrm{c0}})\Delta\tilde{\boldsymbol{\psi}}_{\mathrm{c}} + \alpha_{\psi}\Delta\boldsymbol{\psi}_{\mathrm{c,ref}} \tag{13}$$

where $\tilde{\boldsymbol{\psi}}_{\mathrm{c}} = \boldsymbol{\psi}_{\mathrm{c}} - \hat{\boldsymbol{\psi}}_{\mathrm{c}}$ is the estimation error. The estimation-error dynamics are obtained using (1b), (2), (9), and (13), leading to

$$\frac{\mathrm{d}\Delta\tilde{\boldsymbol{\psi}}_{\mathrm{c}}}{\mathrm{d}t} = -(\boldsymbol{K}_{\mathrm{o0}} + \boldsymbol{J}\omega_{\mathrm{c0}})\Delta\tilde{\boldsymbol{\psi}}_{\mathrm{c}} - \underbrace{\boldsymbol{K}_{\mathrm{o0}}\boldsymbol{J}\boldsymbol{\psi}_{\mathrm{g0}}}_{=\boldsymbol{0}_{2,1}}\Delta\delta \tag{14}$$

where $\boldsymbol{K}_{\mathrm{o0}} = \alpha_{\mathrm{o}}\boldsymbol{\psi}_{\mathrm{g0}}\boldsymbol{\psi}_{\mathrm{g0}}^{\mathrm{T}}/\|\boldsymbol{\psi}_{\mathrm{g0}}\|^2$. The expression for the load angle dynamics is

$$\frac{\mathrm{d}\Delta\delta}{\mathrm{d}t} = \Delta\omega_{\mathrm{c}} - \Delta\omega_{\mathrm{g}} \tag{15}$$

The state-space form is obtained from (13)–(15),

$$\begin{aligned}\dot{\boldsymbol{x}} &= \underbrace{\begin{bmatrix} -\alpha_{\psi}\boldsymbol{I} & \alpha_{\psi}\boldsymbol{I} - \boldsymbol{J}\omega_{\mathrm{c0}} & \boldsymbol{0}_{2,1} \\ \boldsymbol{0}_{2,2} & -\boldsymbol{K}_{\mathrm{o0}} - \boldsymbol{J}\omega_{\mathrm{c0}} & \boldsymbol{0}_{2,1} \\ \boldsymbol{0}_{1,2} & \boldsymbol{0}_{1,2} & 0 \end{bmatrix}}_{\boldsymbol{A}} \boldsymbol{x} + \underbrace{\begin{bmatrix} \alpha_{\psi}\boldsymbol{I} \\ \boldsymbol{0}_{2,2} \\ \boldsymbol{0}_{1,2} \end{bmatrix}}_{\boldsymbol{B}_{\mathrm{c}}} \Delta\boldsymbol{\psi}_{\mathrm{c,ref}} \\ &\quad + \underbrace{\begin{bmatrix} \boldsymbol{0}_{2,1} \\ \boldsymbol{0}_{2,1} \\ 1 \end{bmatrix}}_{\boldsymbol{B}_{\mathrm{m}}} \Delta\omega_{\mathrm{c}} + \begin{bmatrix} \boldsymbol{0}_{2,1} \\ \boldsymbol{0}_{2,1} \\ -1 \end{bmatrix} \Delta\omega_{\mathrm{g}} \end{aligned} \tag{16}$$

where $\boldsymbol{x} = [\Delta\boldsymbol{\psi}_{\mathrm{c}}^{\mathrm{T}}, \Delta\tilde{\boldsymbol{\psi}}_{\mathrm{c}}^{\mathrm{T}}, \Delta\delta]^{\mathrm{T}}$.

The closed-loop transfer functions can be obtained from the system matrices in (16). With the output matrix $\boldsymbol{C}_{\mathrm{c}} = [\boldsymbol{I}, \boldsymbol{0}_{2,2}, \boldsymbol{0}_{2,1}]$, the converter flux dynamics $\Delta\boldsymbol{\psi}_{\mathrm{c}} = \boldsymbol{G}_{\mathrm{c}}(s)\Delta\boldsymbol{\psi}_{\mathrm{c,ref}}$ are obtained, where the transfer function matrix $\boldsymbol{G}_{\mathrm{c}}(s) = \boldsymbol{C}_{\mathrm{c}}(s\boldsymbol{I}_5 - \boldsymbol{A})^{-1}\boldsymbol{B}_{\mathrm{c}} = \alpha_{\psi}/(s + \alpha_{\psi})\boldsymbol{I}$. Furthermore, the output torque is

$$\begin{aligned}\Delta\tau_{\mathrm{g}} &= \boldsymbol{i}_{\mathrm{c0}}^{\mathrm{T}}\boldsymbol{J}\Delta\boldsymbol{\psi}_{\mathrm{c}} - \boldsymbol{\psi}_{\mathrm{c0}}^{\mathrm{T}}\boldsymbol{J}\Delta\boldsymbol{i}_{\mathrm{c}} \\ &= \underbrace{\left(\boldsymbol{i}_{\mathrm{c0}}^{\mathrm{T}}\boldsymbol{J} - \frac{\boldsymbol{\psi}_{\mathrm{c0}}^{\mathrm{T}}\boldsymbol{J}}{L}\right)}_{\boldsymbol{a}^{\mathrm{T}}}\Delta\boldsymbol{\psi}_{\mathrm{c}} + \underbrace{\frac{\boldsymbol{\psi}_{\mathrm{c0}}^{\mathrm{T}}\boldsymbol{\psi}_{\mathrm{g0}}}{L}}_{b}\Delta\delta \end{aligned} \tag{17}$$

Hence, the output matrix corresponding to $\Delta\tau_{\mathrm{g}} = G_{\mathrm{m}}(s)\Delta\omega_{\mathrm{c}}$ is $\boldsymbol{C}_{\mathrm{m}} = [\boldsymbol{a}^{\mathrm{T}}, \boldsymbol{0}_{1,2}, b]$, giving $G_{\mathrm{m}}(s) = \boldsymbol{C}_{\mathrm{m}}(s\boldsymbol{I}_5 - \boldsymbol{A})^{-1}\boldsymbol{B}_{\mathrm{m}} = \boldsymbol{\psi}_{\mathrm{c0}}^{\mathrm{T}}\boldsymbol{\psi}_{\mathrm{g0}}/(sL)$. Other transfer functions can be obtained similarly.

References

[1] R. Rosso, X. Wang, M. Liserre, X. Lu, and S. Engelken, "Grid-forming converters: Control approaches, grid-synchronization, and future trends—a review," *IEEE Open J. Ind. Appl.*, vol. 2, pp. 93–109, Apr. 2021.

[2] D. B. Rathnayake, M. Akrami, C. Phurailatpam, S. P. Me, S. Hadavi, G. Jayasinghe, S. Zabihi, and B. Bahrani, "Grid forming inverter modeling, control, and applications," *IEEE Access*, vol. 9, pp. 114 781–114 807, Aug. 2021.

[3] A. Tayyebi, D. Groß, A. Anta, F. Kupzog, and F. Dörfler, "Frequency stability of synchronous machines and grid-forming power converters," *IEEE Trans. Emerg. Sel. Topics Circuits Syst.*, vol. 8, no. 2, pp. 1004–1018, June 2020.

[4] S. A. Khan, M. Wang, W. Su, G. Liu, and S. Chaturvedi, "Grid-forming converters for stability issues in future power grids," *Energies*, vol. 15, no. 14, July 2022.

[5] J. Matevosyan, B. Badrzadeh, T. Prevost, E. Quitmann, D. Ramasubramanian, H. Urdal, S. Achilles, J. MacDowell, S. H. Huang, V. Vital, J. O'Sullivan, and R. Quint, "Grid-forming inverters: Are they the key for high renewable penetration?" *IEEE Power Energy Mag.*, vol. 17, no. 6, pp. 89–98, Nov./Dec. 2019.

[6] G.-S. Seo, M. Colombino, I. Subotic, B. Johnson, D. Gros, and F. Dorfler, "Dispatchable virtual oscillator control for decentralized inverter-dominated power systems: Analysis and experiments," in *Proc. IEEE APEC*, Anaheim, CA, USA, Mar. 2019, pp. 561–566.

[7] A. Alassi, K. Ahmed, A. Egea-Alvarez, and O. Ellabban, "Performance evaluation of four grid-forming control techniques with soft black-start capabilities," in *Proc. ICRERA*, Glasgow, U.K., Sept. 2020, pp. 221–226.

[8] A. Alassi, K. Ahmed, A. Egea-Alvarez, and C. Foote, "Modified grid-forming converter control for black-start and grid-synchronization applications," in *Proc. UPEC*, Middlesbrough, U.K., Sept. 2021.

[9] N. Pogaku, M. Prodanovic, and T. C. Green, "Modeling, analysis and testing of autonomous operation of an inverter-based microgrid," *IEEE Trans. Power Electron.*, vol. 22, no. 2, pp. 613–625, Mar. 2007.

[10] K. De Brabandere, B. Bolsens, J. Van den Keybus, A. Woyte, J. Driesen, and R. Belmans, "A voltage and frequency droop control method for parallel inverters," *IEEE Trans. Power Electron.*, vol. 22, no. 4, pp. 1107–1115, July 2007.

[11] M. Guan, W. Pan, J. Zhang, Q. Hao, J. Cheng, and X. Zheng, "Synchronous generator emulation control strategy for voltage source converter (VSC) stations," *IEEE Trans. Power Syst.*, vol. 30, no. 6, pp. 3093–3101, Nov. 2015.

[12] A. Moulichon, M. Alamir, V. Debusschere, L. Garbuio, M. A. Rahmani, M.-X. Wang, and N. Hadjsaid, "Observer-based current controller for virtual synchronous generator in presence of unknown and unpredictable loads," *IEEE Trans. Power Electron.*, vol. 36, no. 2, pp. 1708–1716, Feb. 2021.

[13] L. Zhang, L. Harnefors, and H.-P. Nee, "Power-synchronization control of grid-connected voltage-source converters," *IEEE Trans. Power Syst.*, vol. 25, no. 2, pp. 809–820, May 2010.

[14] L. Harnefors, M. Hinkkanen, U. Riaz, F. M. M. Rahman, and L. Zhang, "Robust analytic design of power-synchronization control," *IEEE Trans. Ind. Electron.*, vol. 66, no. 8, pp. 5810–5819, Aug. 2019.

[15] L. Harnefors, F. M. M. Rahman, M. Hinkkanen, and M. Routimo, "Reference-feedforward power-synchronization control," *IEEE Trans. Power Electron.*, vol. 35, no. 9, pp. 8878–8881, Sep. 2020.

[16] L. Tiitinen, M. Hinkkanen, J. Kukkola, M. Routimo, G. Pellegrino, and L. Harnefors, "Stable and passive observer-based V/Hz control for synchronous motors," in *Proc. IEEE ECCE*, Detroit, MI, Oct. 2022.

[17] M. Marwali and A. Keyhani, "Control of distributed generation systems-part i: Voltages and currents control," *IEEE Trans. Power Electron.*, vol. 19, no. 6, pp. 1541–1550, Nov. 2004.

[18] E. Rokrok, T. Qoria, A. Bruyere, B. Francois, and X. Guillaud, "Transient stability assessment and enhancement of grid-forming converters embedding current reference saturation as current limiting strategy," *IEEE Trans. Power Syst.*, vol. 37, no. 2, pp. 1519–1531, Mar. 2022.

[19] I. Sadeghkhani, M. E. Hamedani Golshan, J. M. Guerrero, and A. Mehrizi-Sani, "A current limiting strategy to improve fault ride-through of inverter interfaced autonomous microgrids," *IEEE Trans. Smart Grid*, vol. 8, no. 5, pp. 2138–2148, Sept. 2017.

[20] M. Hinkkanen, S. E. Saarakkala, H. A. A. Awan, E. Mölsä, and T. Tuovinen, "Observers for sensorless synchronous motor drives: Framework for design and analysis," *IEEE Trans. Ind. Appl.*, vol. 54, no. 6, pp. 6090–6100, Nov./Dec. 2018.

[21] J. Kukkola, M. Routimo, M. Hinkkanen, and L. Harnefors, "A voltage-sensorless controller for grid converters," in *Proc. IEEE PES ISGT Europe*, Espoo, Finland, Oct. 2021.